

**TRANSIENT TRACER-CONCENTRATION COVARIANCE PATTERNS IN SINGLE-SUBJECT
[¹⁵O]WATER DYNAMIC PET: A FINGER MOVEMENT STUDY**

J.J. Moreno-Cantú^{1,3}, J-S. Liow^{1,3}, J. Anderson³, D.A. Rottenberg^{1,2,3}, S.C. Strother^{1,2,3}.

Departments of ¹Radiology and ²Neurology, University of Minnesota; and ³PET Imaging
Service, Veterans Affairs Medical Center, Minneapolis, Minnesota, U.S.A.

Address correspondence to:

Jeih-San Liow Ph.D.
PET Imaging Service (11P)
VA Medical Center
One Veterans Dr.
Minneapolis, MN. 55417
U.S.A.

Telephone: (612) 725-2000 ext. 4789
Fax: (612) 725-2068
E-mail: jsl @pet.med.va.gov

Running Title: Covariance patterns of dynamic O-15 PET

Keywords: . PET, Activation, Principal Component Analysis, Canonical Variable
Analysis, Time series, Consensus Alignment, Normalization

ABSTRACT

In this study, we identify patterns of tracer-concentration covariance in time series from single-subject PET studies using principal component and canonical variable analyses (PCA/CVA). Single-subject [^{15}O]water bolus time-series were collected in a fashion similar to that of fMRI experiments and used to identify patterns that cannot be detected with static [^{15}O]water PET. The study was carried out on six normal volunteers performing alternating control and activation task (quiet rest and finger-to-thumb opposition). Each bolus time-series consisted of nine successive 10-sec scans performed 20 sec after a bolus injection. Four activation and four baseline bolus time-series were collected for each subject. PCA and CVA were performed on data sets from individual subjects and the findings were compared against results from previously reported fMRI and static PET investigations of this activation task. We demonstrate that the multivariate analysis of fast dynamic PET data without explicit scan normalization provides a new data-driven normalization procedure that yields consistent and readily interpretable results across individual subjects. In addition, intra-subject alignment using a fixed reference volume was found to be unreliable due to noise in the dynamic scans. This problem was overcome by using a consensus alignment procedure. Our results demonstrate that PET [^{15}O]water activation studies acquired in a dynamic fashion and analyzed using multivariate techniques can identify pre-processing artifacts and vascular confounds similar to those seen in fMRI while reliably extracting covariance patterns related to tracer physiology and the activation task in individual subjects.

INTRODUCTION

Over the past ten years, technical advances in the field of functional Magnetic Resonance Imaging (fMRI) have propelled this technique to the forefront of the existing functional neuroimaging modalities [Belliveau et al., 1991; Kwong et al., 1992; Turner et al., 1997]. At the same time, [^{15}O]water PET imaging, which was the leading neuroimaging technique during the late 80's and early 90's, has lost much of its cutting-edge status. fMRI is claimed to be superior to [^{15}O]water PET because of its higher spatial and temporal resolution [Turner et al., 1997]. Studies using fMRI are also less expensive than those using [^{15}O]water PET, and since no known risks are associated with fMRI procedures, the number of scans collected from any given subject is not constrained by concerns regarding the subjects's safety. Thus, in a typical functional neuroimaging session, more fMRI scans than static PET scans can be collected and therefore fMRI data sets have usually much larger nominal degrees of freedom than those obtained with traditional [^{15}O]water PET [Turner et al., 1997; Kinahan and Noll, 1999]. Nevertheless, direct comparisons of signal and noise levels between [^{15}O]water PET and fMRI remain difficult to make because of technical issues which have yet to be fully addressed [e.g., Zaini et al., 1999]. That fMRI is perceived to be an imaging technique more accessible and superior to [^{15}O]water PET by most investigators is demonstrated by the difference in the number of neuroimaging research groups using fMRI and PET. For instance, at the *1999 Conference on Functional Mapping of the Human Brain (section Methods/Physiology/Cognition)*, the number of abstracts reporting fMRI results was 3.5 times greater than the number of abstracts reporting PET results [Toga et al., 1999].

Advocates of [^{15}O]water PET argue that PET should remain the technique of choice if simultaneous data collection from the entire brain is desired and image artifacts (in brain regions such as the inferior temporal, cerebellar or mesial anterior frontal cortices) are to be avoided, or if the experimental protocol requires free access to the subject during data collection. The latter is an important advantage particularly when monitoring high-order cognitive tasks. In PET experiments, subjects can easily speak, write, manipulate objects, point at things, etc. Furthermore, since the brain's hemodynamic response governed by the physiology of the BOLD signal is on the order of 5 - 10 seconds in a 3 - 5 mm region of tissue [Malonek and Grinvald, 1996], the temporal resolution of [^{15}O]water PET may only need to be increased to 5 - 10 sec to be comparable to typical whole-brain BOLD fMRI techniques. Moreover, the recent commercial trend to couple axial-computed tomography (CT), which yields high-resolution structural images with emission tomography [Beyer et al., 2000] is likely to prompt the development of PET scanners with spatial resolution higher than that obtainable with PET-only tomographs. Current PET scanners have a spatial resolution in the 2 - 4 mm range [Schmand et al., 1999]; which is already comparable to that of whole-brain BOLD fMRI studies.

In this investigation, we explored the possibility of improving the temporal resolution of the [^{15}O]water PET technique by using multivariate statistical analysis to extract transient signal patterns from single-subject PET images collected in a manner similar to that employed in fMRI studies (i.e., as time series consisting of runs of successive scans, with each scan lasting a few seconds). This approach has been used successfully to extract signal patterns in fMRI, dynamic FDG and static [^{15}O]water PET [Strother et al., 1996; Wu

et al., 1996; Liow et al., 2000]. We argue that analyzing [^{15}O]water PET images acquired as dynamic time-series can significantly enhance the ability of PET scanners to detect transient signals. This is of particular importance for the many centers with established PET imaging protocols. We extend the work of Andersson [1998] and demonstrate that group averaging and the prevalent 40-120 sec scan integration times are more of a customary practice than a requirement of the PET imaging technique. We set out to determine if principal-component analysis (PCA) and canonical-variable analysis (CVA) can be used to extract transient patterns of tracer concentration, previously undetected in quasi-static [^{15}O]water PET measurements with the commonly used integration time of 40 to 120 seconds. We speculate that, if the acquisition and analysis techniques described in this study are employed with isotopes such as ^{14}O or ^{10}C , which have half-lives 41% and 85% shorter than ^{15}O , respectively, the effectiveness of PET for functional neuroimaging studies may be improved significantly [Sajjad et al., 2000; Law et al., 2000].

Terminology. 1) *Scan*: a 10-sec integration of the concentration of tracer in the brain; 2) *Run*: a collection of independent scans acquired consecutively following a single bolus-injection of tracer; a bolus time series, 3) *Scanning session*: the uninterrupted period required to collect all the runs for a given subject; and 4) *Image volume*: the collection of 2D images forming a 3D map (volume) of the concentration of tracer in the brain resulting from the reconstruction of 3D PET scans.

MATERIALS AND METHODS

Subjects and Tasks

Six volunteers (4 male, 2 females; aged: 24-45 years) were scanned after written informed consent was obtained in accordance with a protocol approved by the Minneapolis VA Medical Center's Institutional Review Board. All female subjects of child bearing age had a pre-scan serum pregnancy test. Each scanning session consisted of eight runs with alternating control (resting quietly with eyes covered and ears plugged) and activation states. During the activation runs, subjects were asked to perform a finger-opposition task consisting of sequential opposition of the left thumb and successive digits (2,3,4,5,4,3,2,3...), externally paced with a 1 Hz auditory signal.

Data Acquisition and Preprocessing

All PET scans were acquired with a Siemens ECAT 953B-31 scanner operating in 3D mode (10.8 cm axial field of view, with reconstructed in-plane and axial resolution of 8.5 mm and 6 mm respectively [Liow et al., 1997], on a 128 x 128 x 31 grid with 3.125 x 3.125 x 3.375 mm³ voxels). Tracer delivery, task execution and data collection for each run are depicted in Fig. 1. Each tracer injection consisted of 13 mCi of [¹⁵O]water infused as a bolus of 6.2 ml sterile saline at the speed of 1 ml / sec [Palmer et al., 1995]. Data collection started 20 sec after injection to allow the radiotracer to arrive in the brain and lasted 90 sec. Task execution and stimulus presentation began concurrently with tracer injection and lasted 60 sec - they were stopped 40 seconds after the start of data

collection in order to maximize the signal-to-noise ratio (SNR) [Cherry et al., 1995; Moreno-Cantú et al., 1998]. Following each injection, data were collected in one run formed by nine 10 sec scans. PET counts were corrected for deadtime, randoms and attenuation, and were reconstructed using 3D filtered backprojection. The cerebellar signal, which was prominent in previous studies [e.g., Strother et al., 1995], was not analyzed here since the cerebellum could not be imaged consistently across subjects because of the limited axial field of view of our scanner (10.8 cm).

Intra-Subject Alignment

Due to the poor counting statistics observed in the scans acquired immediately after bolus injection, two image alignment algorithms were tested in order to explore the effect that mis-registration artifacts might have on PCA/CVA of runs from individual subjects. The two image alignment algorithms are referred to here as the standard and consensus algorithms. They each employed a commonly used 6-parameter rigid-body transformation (AIR 3.0) to generate a session-mean volume [Woods et al., 1998]. The session-mean volume was then used to obtain a 12-parameter affine transformation to a simulated PET template in Talairach space. All scans were resampled into Talairach space using combined intra- and inter-session transformations in a single operation [Strother et al., 1994, 1995]. To reduce the impact of possible misalignment artifacts on the PCA/CVA analysis, a $3 \times 3 \times 3$ - voxel boxcar filter was applied to the image volumes prior to resampling (a $2D\ 3 \times 3$ filter was used for the end slices). The alignment was performed on intra-cerebral voxels, which were determined by thresholding each slice at 45% of its maximum value.

Consensus Alignment. Six-parameter rigid-body transformation matrices were obtained for all possible scan pair combinations from a subject using AIR 3.0 (i.e., $S_i \rightarrow (T_{ij}) \rightarrow S_j$ where i, j are any of $(9 \text{ scans/run}) \times (8 \text{ runs/subject}) = 72 \text{ scans}$). The transformation matrices (T_{ij}) were then used to obtain a consensus transformation by averaging the 4×4 homogeneous coordinate products, $T_{ij}^k = T_{ik}T_{kj}$, over all scans (k) to form the average matrix $\langle T_{ij}^k \rangle_k$. The average transformation matrix was then converted to a six-parameter rigid body transformation matrix by using $\langle T_{ij}^k \rangle_k$ to convert an evenly spaced $20 \times 20 \times 20$ point grid covering the average brain mask and then calculating the six-parameter Procrustes transformation of the original to the transformed grid; **Standard alignment.** A single scan (S_r) from one of the four control runs from a subject was selected as a reference (based on counting statistics). AIR 3.0 was used to generate a rigid-body transformation matrix for each of the remaining 71 scans (i.e., $S_i \rightarrow (T_{ir}) \rightarrow S_r$ where i is any of $[(9 \text{ scans/run}) \times (8 \text{ runs/subject}) - (1 \text{ reference scan})] = 71 \text{ scans}$).

Image Normalization

The effects of image normalization on the ability of PCA and CVA to extract activation patterns was investigated by comparing the principal components (PCs) and canonical variables (CVs) obtained from the analysis of image volumes normalized by two different methods. The first method involved dividing each image by the mean of its intracerebral voxel values. This method, referred to as volume-mean normalization (VMN), is commonly used for the analysis of PET functional neuroimaging data [e.g., Muley et al., 2001]. The second method involves no explicit mean adjustment prior to the analysis. However, after PCA the first principal component (PC1) was dropped before the

subsequent CVA; this component was identified as variance largely due to tracer uptake in the tissue contributing differential gray-white tissue scaling effects. This elimination of variance unrelated to the CVA class structure (see below) is similar to VMN but produces an improved outcome (see Results).

PCA on [¹⁵O]water PET Time Series

We applied PCA to the 72 images from each subject (8 x 9 scans) to investigate temporal and spatial activity-concentration covariance patterns in within-subject runs. For each subject, PCA was performed four times, i.e., for each of the pre-processing protocols previously described. Thus, PCA was performed on images with and without VMN normalization, and aligned using either the standard or consensus alignment algorithms. The resulting PCs were then compared in order to evaluate the ability of PCA to detect brain function across pre-processing protocols. In order to remove variance due to subject-specific effects from the data, the mean image volume from each subject (i.e., each session) was subtracted from the individual image volumes. This helped to reduce extraneous variance and concentrate the bolus time-series changes in the first few PCs from PCA. For each subject and each pre-processing protocol, a data matrix was created, consisting of 72 rows (one image volume/row) and columns defined by the number of voxels within the intersection volume of all subjects' brain masks. PCA was then used to decompose the data matrices into orthogonal eigenvectors and associated eigenimages [Jackson, 1991].

PCA/CVA on [¹⁵O]water PET Time Series

To perform a flexible exploratory CVA capable of separating the bolus time effects from activation/control differences, we specified 18 classes: 9 for activation runs and 9 for control runs [e.g., Strother et al., 1996; Friston et al., 1996; Kustra and Strother 2001]. Based on the identification of interpretable PCs and artifacts from the PCA of data sets for each of the four pre-processing protocols, we focussed on PCA/CVA results with consensus alignment and without VMN normalization, which produced robust interpretable components with minimal artifacts. PCs 2 -10 (data was normalized by dropping PC1) were entered into CVA to identify canonical eigenvectors which successively maximize the variance ratio of the between-class mean and within-class covariance structure and their associated canonical eigenimages. Given the 18 classes, there are 17 possible orthogonal canonical eigenvectors or discriminant functions (i.e., linear combinations of weighted PCs and associated eigenimages) [Mardia et al., 1979]. In this study, only spatial and temporal covariance patterns of effects identified as significant canonical dimensions defined by Bartlett's adjusted chi-square test [Mardia et al., 1979] will be discussed and compared across the six subjects.

RESULTS

Image Alignment

The comparison of PCA findings across the two alignment techniques suggests that PCA consistently identified and isolated the variance introduced by mis-registration in individual PCs. This is an important finding because mis-registration artifacts are likely to be present when analyzing PET runs since individual scans are susceptible to high noise levels introduced by low counting statistics. The mis-registration artifacts appear as regions of high variance along the brain boundaries. In our experiment, significant artifacts were identified in individual PCs in each of the six subjects. Fig. 2 illustrates these findings. The figure depicts eigenimages associated with PCs 2 and 3 for the non-normalized data using standard alignment from Subject 5. Prominent edge artifacts are present in both images. The average magnitude of misregistration using standard alignment was about the same (by comparing the sum of the variance of all PCs that demonstrate this artifact) in both VMN and non-normalized data sets, relatively large and spread across several early PCs in all subjects. In the VMN data, half the subjects showed artifacts in PC1 (the largest source of variance in the data), while the others had artifacts beginning in PC2. In the non-normalized data mis-registration artifacts only began to appear in PC2 because tracer uptake and washout in brain tissue appears to constitute the largest source of variance, which is captured by PC1. In contrast to the results obtained with the consensus alignment, where mis-registration artifacts were seen only in one subject's non-normalized data, the standard alignment procedure produces mis-registration

artifacts in all the subjects regardless of whether or not normalization was used. This finding demonstrates that the standard alignment technique performs poorly when aligning noisy images.

Image Normalization

Image normalization was found to be an unnecessary pre-processing step when data sets are analyzed using PCA. This finding was observed across all the subjects and for both image registration techniques that were tested. Absence of normalization allowed PCA to isolate the variance associated with task execution in fewer, more reproducible components. Figures 3 and 4 illustrate the first 6 PCs from Subject 5 with and without VMN normalization, respectively. Both analyses used the consensus alignment. In the VMN data, PC1 contains a vascular response resembling the shape of the vascular input function (Fig. 3A). PC2 and PC3 appear to capture the pattern of tracer uptake and washout in brain tissue. PC2-PC6, which are strongly influenced by outliers, display varying amounts of activation/control differences. With VMN normalization, PCA outliers occurring in the early low-count scans were a consistent feature across all subjects. In the non-normalized data, PC1 captures the tracer uptake and washout in tissue (Fig. 4A). The vascular response appears to be in PC2 (Fig. 4B), with a shape similar to that in Fig. 3A. The activation/control effect is concentrated in PC3 with a temporal trend that is more variable in the baseline than the activation state.

PCA on [¹⁵O]water PET Time Series

Compared to non-normalized data, VMN produces outliers with the activation/control effect spread across several PCs, which makes the interpretation of the different components and effects more difficult. For the rest of this paper, we will focus on results with consensus alignment and without VMN normalization, which produced robust readily interpretable components in all subjects. To interpret the tracer behaviour characterized by each PC, the spatial distribution of relative voxel weights in the eigenimages associated with each PC must also be examined. Figure 5 illustrates selected eigenimages associated with PCs 1-3 of the non-normalized data in Fig. 4 superimposed on our MRI reference volume. The PCs and their corresponding eigenimages from this single-subject analysis are interpreted as follows. (Note that changes in counts per voxel are obtained by multiplying the voxel weights in Fig. 5 by the scan weights in Fig. 4).

PC1

For both activation and control trials, the weights in Fig. 4A demonstrate a rapidly rising signal in the first two or three scans (20 – 30 sec) that peaks between the second and fourth scans and then decreases to values similar to the first scan. This PC closely resembles the shape of a typical [¹⁵O]water time activity curve (TAC) in brain tissue, capturing the variance introduced by tracer arrival in the brain, its dispersion and decay. This conclusion is supported by the global structure of the eigenimage (Fig. 5A, plane 27-33) with a strong correlation between grey matter (GM; white to yellow orange), and white matter (WM; orange to black).

PC2

The focal brain regions with large positive weights (red), which co-vary in the eigenimage patterns (Fig. 5B), exhibit count levels that start relatively high and decrease exponentially, reaching a plateau towards the end of the run (Fig 4B). Again, the individual bolus time series do not exhibit obvious activation/control differences. The highest voxel weights in this eigenimage match the anatomy of brain regions served by the anterior and middle cerebral arteries (Fig. 5B, planes 27 - 33). The large peak values found bilaterally around the primary auditory cortices are over regions where heavy branching of the middle cerebral artery occurs [Heimer, 1994]. We believe that PC2 demonstrates predominantly the vascular response to delivery of the bolus (input function). Since data collection started 20 seconds after the 6-second bolus infusion began (6 ml at 1 ml / sec), the monotonic decrease in activity indicates that data collection started at or shortly after arrival of activity in the brain. Although not shown here, subtle activation/control differences were detected in this component in three of the six subjects. This suggests that subtle, task dependent vascular effects may contaminate PET activation studies in a manner similar to the remote large vessel effects reported in fMRI. [Segebarth et al., 1994; Kim and Ugurbil, 1997].

PC3

The variance represented by this component exhibits clear activation/control differences (Fig. 4C). The highest voxel weights in the eigenimages are located in the right primary motor cortex (M1) and supplementary motor area (SMA) (Fig. 5C, plane 39 - 41). This indicates that PC3 captures temporal co-variation across brain regions associated with

execution of the task. The finding is in agreement with results from previous PET and fMRI studies [e.g., Strother et al., 1995, Tegeler et al., 1999]. The peak contrast between activation and control conditions occurs during the second and third scans, i.e., when the tracer concentration is highest in the brain's GM as illustrated in PC1 (Figs. 4A and 4C) and in agreement with our understanding of the tissue response in [^{15}O]water studies [Cherry et al., 1995, Moreno-Cantú et al., 2000]. Note that in addition to the remote vascular effects in PC2, PET bolus time-series also suffer from vascular confounds with large variances in activation regions in a manner that is analogous to fMRI (e.g., Tegeler et al., 1999). In Figure 5B, slice A41, there is a strong vascular response in the right SMA, which completely overlaps with the activation response in that area (slice B41).

PCs 4 and higher

None of these PCs showed a consistent correlation with either task execution or the nine bolus time-series scan weights (Fig. 4D – 4F). The time courses indicate that PC4 may reflect interaction between task (PC3) and specific bolus injections, with more variability in control than in activation runs (also seen in PC3). However, no readily interpretable spatial patterns were observed in the eigenimages. Similar results were obtained for the other five subjects except that minor activation/control differences were observed in PCs 4 and 5 for one subject and in PC5 for another subject.

PCA/CVA on [^{15}O]water PET Time Series

In situations where PCA fails to partition variance from different effects into interpretable individual components, CVA can be applied to a subset of PCs to create a

form of noise-informed PCA that may provide more interpretable components based on an explicitly assigned class structure (e.g., activation/control conditions and/or temporal scan sequences). To reduce potential noise confounds caused by the large amount of variance due to tissue uptake in PC1, we “normalized” our data by excluding PC1; only PCs 2-10 were used as input to CVA. For the six subjects, the variance accounted for by PC1 ranges from 64% - 89% compared to that from PC2, which ranges from 0.76% - 2.3%. Figure 6 illustrates the mean and range (shaded region) of PC1 for the activation and control runs from all six subjects. The tightness of the range, its resemblance to tissue uptake and washout curves, and the distribution of positive eigenimage weights throughout gray and white matter (Fig, 5A) strongly support the conclusion that this PC represents the large-scale confounds that VMN attempts to remove with a single spatially-independent scaling factor. For each of the six subjects, only two significant CVA dimensions were identified corresponding to two uncorrelated time courses for the class means, i.e., temporal evolution within bolus time series. Canonical variables of each significant dimension (CV1: $\chi^2 = 371 - 460$, $df = 153$; CV2: $\chi^2 = 190 - 252$, $df = 128$, both $p < 0.001$) are depicted in Fig. 7 as mean-activation and -control bolus time series for each subject. CV1 (Fig. 7A) resembles the vascular response seen in PC2 (cf., Fig. 4B). All 6 subjects demonstrate small but consistent activation/control differences in the vascular response, with all but Subject 6 having a higher peak for activation runs than for control runs (Fig. 7A). This, again, suggests that there may be a task dependent interaction between the vascular components and task specific activation in a manner analogous to large vessel effects seen in fMRI. CV2 resembles the activation/control effect seen in PC3 (cf., Fig. 4B). The activation signal seen in the scan weights is largest in the early phase of the run

(scans 1 – 4) when the tracer concentration gradient in the brain is steep, and gradually diminishes towards the end as the concentration gradient levels out (Fig. 7B). Figure 8 illustrates canonical eigenimages corresponding to CV1 and CV2 for Subject 5. The highest voxel weights for the two canonical eigenimages are in the same regions as in eigenimages associated with PCs 2 and 3 (Figs. 5B) respectively. (CV1 and CV2 are heavily dependent on linear combinations of PC2 and PC3.) The similarity of the activation patterns is demonstrated by the relatively high correlation between the two eigenimages associated with CV2 and PC3. Five of the six subjects yield voxel-to-voxel scatter plot correlation coefficients > 0.85 between the two eigenimages; only Subject 1 yields a lower correlation coefficient of 0.68. The canonical eigenimages in Fig. 8 display an enhanced vascular response compared with Fig. 5B, (slice 39 – 40) that now includes a component in the primary motor region.

DISCUSSION

When analyzing PET [^{15}O]water scans obtained with short dynamic frames in single subjects without normalization, PCA is capable of detecting tracer concentrations that reflect the global tissue uptake and dispersion pattern, a regional vascular response, and task-dependent temporal changes in localized regions. Using PCA without a priori knowledge, these effects were consistently identified in separate PCs across all six subjects provided we removed confounding variance sources due to poor alignment and normalization artifacts in low count scans. Nevertheless, because of the nonspecific nature of orthogonal variance decompositions, it is likely that the true signal structure of different effects is still spread across multiple PCs either due to the non-orthogonal, coupled nature of the effects themselves or large differences in effect magnitude, e.g., tissue uptake versus activation/control effects. Therefore, to further optimize the separation of effects of interest, we analyzed the PCs with a “noise-informed PCA” based on CVA and an exploratory class structure that allowed arbitrary time-series effects to be discovered as a function of control and activation brain states. Moreover, to eliminate the largest variance unrelated to effects of interest, we applied a simple data-driven normalization by discarding PC1 before CVA, thereby avoiding many of the problems associated with normalizing PET scans [Andersson, 1997].

For the non-normalized PCA data, we have demonstrated that PC1 (Fig.4A) accounts for 37 to 127 times the next largest source of variance in single-subject PCAs and consistently represents the TAC. This justified the exclusion of PC1 in the subsequent CVA. In several subjects, PC1 did show a small contribution to either the vascular effect

or the activation/control effect when it was included in the CVA. This could indicate that either some coupling between tissue uptake and the activation/control effect does exist, or that variance from PC1 “leaks” into other PCs due to noise and/or the significantly larger variance for PC1 relative to other PCs. This phenomenon has been observed with multivariate analysis in fMRI where removal of physiological noise sources was found to dramatically improve the analysis results compared to simple t - tests [Tegeler et al., 1999]. Our single-subject PET results contained activated foci that were consistent with those described in previous group-PET and single-subject fMRI experiments for the same motor task [Strother et al., 1995, Tegeler et al., 1999]. The activation signal in M1 was the strongest and most consistent across subjects, whereas the activation signal in SMA was weaker and was detected in only some of the subjects.

More sophisticated strategies for selecting PCs as input to CVA are currently being developed [Kustra and Strother, 2001], and other basis choices such as independent component analysis might provide a better initial separation of effects. Clustering provides a related procedure that is being used to analyze PET [e.g., Ashburner et al., 1996] and fMRI time series [Goutte et al., 1999]. However, we believe that clustering has the disadvantage that it creates a segmentation in which each voxel may be assigned to one and only one time course. At PET and probably fMRI resolution levels this makes it impossible for clustering techniques to identify mixed vascular and tissue activation effects of the kind illustrated in the primary motor region in Fig. 8.

Our results also demonstrate that the absence of explicit normalization (e.g., VMN) removes artifacts, allowing PCA to reliably isolate the variance associated with task

execution in a smaller number of PCs. Although a decrease in the number of task-dependent PCs is not essential, since CVA may still be used to achieve separation of the effects of interest, we believe that this reduction in the number of effect-specific PCs is beneficial for two reasons. First, all PCs were easier to interpret without normalization, and individual components were more consistent across subjects. In this data set PC3 always accounted for the most variance associated with task execution. Second, images acquired with short dynamic scans can be quite different due to the rapidly changing tracer kinetics, and these differences are not adequately removed by dividing each scan using a single number as in volume mean normalization. This may explain why the PCA results in the VMN data were more complicated and difficult to interpret. Without explicit normalization, the physiological effect that accounts for the most variance – the tissue TAC – was well separated out by PCA as a single component. This spatially-dependent source of variance can simply be dropped in the subsequent CVA analysis as an alternative to the spatially-independent subject scaling factor of the scaled subprofile model [Moeller and Strother, 1991], VMN normalization or more complex iterative techniques [Strother et al., 1995, Andersson, 1997]. Our results provide further evidence that an inappropriate normalization model can be detrimental. On the other hand, a data driven multivariate analysis which does not impose a particular model can achieve a form of implicit normalization by separating the unwanted variance from the “good” variance associated with the desirable effect(s). These advantages may be expected primarily in the early scans of a run when image counts are low but the signals are near peak values [Silbersweig et al., 1993; Moreno-Cantú et al., 2000].

We have also demonstrated that adding a time variable to the sampling of [¹⁵O]water PET data in a fashion similar to the collection of fMRI time series increases the amount of information related to brain function that can be extracted. We speculate that further improvements in temporal resolution of PET activation studies can be achieved with [¹⁴O]water experiments (half-life 70 seconds) performed with a PET scanner capable of acquiring continuous scans for a few seconds per scan, and analyzed with multivariate techniques such as PCA/CVA.

CONCLUSIONS

For PET [^{15}O]water activation studies acquired in a dynamic fashion and analyzed using multivariate techniques, covariance patterns related to the tracer physiology, the activation task, and pre-processing artifacts can be extracted and identified in individual subjects. Analysis of fast dynamic data without explicit scan normalization provides a new data-driven normalization procedure that yields more interpretable results and better reproducibility across subjects. Intra-subject alignment using a fixed reference volume was found to be unreliable due to noise in the dynamic data and was replaced by a consensus alignment procedure. Our results demonstrate that multivariate analysis of [^{15}O]water PET time series increases the information about brain function available from PET activation experiments.

ACKNOWLEDGMENTS

We are grateful to the technical staff from the PET Imaging Service of the Minneapolis VA Medical Center for their assistance during the acquisition and analysis of the PET data sets. This work was supported by the National Institutes of: MH57180 and NS33721.

REFERENCES

- Ashburner J, Haslam J, Taylor C, Cunningham VJ, Jones T. 1996. A cluster analysis approach for the characterization of dynamic PET data. In: Myers R et al., editor. Quantification of Brain function Using PET. San Diego: Academic Press, P253-257.
- Andersson JLR. 1997. How to estimate global activity independent of changes in local activity. *Neuroimage* 6:237-244.
- Andersson JLR 1998. Within-study repeated measurements to increase sensitivity for positron emission tomography activation studies. *J Cereb Blood Flow Metab* 18:319-331.
- Belliveau JW, Kennedy DN Jr, McKinstry RC, Buchbinder BR, Weisskoff RM, Cohen MS, Vevea JM, Brady TJ, Rosen BR. 1991. Functional mapping of the human visual-cortex by magnetic-resonance-imaging. *Science* 254:716-719.
- Beyer T, Townsend DW, Brun T, Kinahan PE, Charron M, Roddy R, Jerin J, Young J, Byars L, Nutt R. 2000. A combined PET/CT scanner for clinical oncology. *J Nucl Med* 41:1369-1379.
- Cherry SR, Woods RP, Doshi NK, Banerjee PK, Mazziotta JC 1995. Improved signal-to-noise in PET activation studies using switched paradigms. *J Nucl Med* 36:307-314.
- Friston KJ, Poline JB, Holmes AP, Frith CD, Frackowiak RSJ. 1996. A multivariate analysis of PET activation studies. *Human Brain Mapping* 4:140-151.
- Goutte C, Toft P, Rostrup E, Nielsen FA, Hansen LK. 1999. On clustering fMRI time series. *Neuroimage*. 9:298-310
- Heimer L. 1994. The human brain and spinal cord. New York: Springer-Verlag. 506p.
- Jackson JE. 1991. A Users Guide to Principal Components. New York, John Wiley & Sons
- Kim S-G, Ugurbil K. 1997. Functional magnetic resonance imaging of the human brain. *J Neuroscience Methods*. 74:229-243.
- Kinahan PE, Noll DC. 1999. A direct comparison between whole-brain PET and BOLD fMRI measurements of single-subject activation response. *Neuroimage* 9:430-438.
- Kustra R, Strother SC. 2001. Penalized discriminant analysis of [¹⁵O]water PET brain images with prediction error selection of smoothing and regularization hyperparameters. *IEEE Trans Med Imaging* (in press).
- Kwong KK, Belliveau JW, Chesler DA, Goldberg IE, Weisskoff RM, Poncelet BP, Kennedy DN Jr, Hoppel BE, Cohen MS, Turner R et al. 1992. Dynamic magnetic resonance imaging of human brain activity during primary sensory stimulation. *Proc Natl Acad Sci* 89:5675-5679.

- Law I, Jensen M, Holm S, Nickles RJ, Paulson OB. 2000. Characterizing the single-subject stimulus frequency dependence in human visual cortex by carbon-10 dioxide and PET. *J Nucl Med Supplement* 41:214P.
- Liow J-S, Strother SC, Rehm K, Rottenberg DA. 1997. Improved resolution for PET volume Imaging through three-dimensional iterative reconstruction. *J Nucl Med* 38:1623-1630.
- Liow J-S, Anderson JR, Strother SC. 2000. Comparing reconstruction algorithms using a multi-variate analysis. *IEEE Trans Nucl Sci* 47:1136-1142.
- Malonek D, Grinvald A. 1996. Interactions between electrical activity and cortical micro-circulation revealed by imaging spectroscopy - implications for functional brain mapping. *Science* 272:551-554.
- Mardia KV, Kent JT, Bibby JM. 1979. *Multivariate analysis*. San Diego: Academic Press. 518p.
- Moeller JR, Strother SC. 1991. A regional covariance approach to the analysis of functional patterns in positron emission tomographic data. *J Cereb Blood Flow Metab* 11:A121-A135.
- Moreno-Cantú JJ, Reutens DC, Thompson CJ, Zatorre RJ, Klein D, Meyer E, Petrides M. 1998. Signal-enhancing switched protocols to study higher-order cognitive tasks with PET. *J Nucl Med* 39:350-356.
- Moreno-Cantu JJ, Liow J-S, Sajjad M, Rottenberg DA, Strother SC. 2000. Reexamining the correlation between [¹⁵O]H₂O delivery and signal size: towards shorter more efficient PET sessions. In: Gjedde A et al. , editor. *Physiological Imaging in the Brain with PET*. San Diego: Academic Press, P289-294.
- Muley SA, Strother SC, Ashe J, Frutiger SA, Anderson JR, Sidtis JJ, Rottenberg DA. 2001. Effects of changes in experimental design on PET studies of isometric force. *Neuroimage* in press.
- Palmer, B. M., Sajjad, M., Rottenberg, D. A. 1995. An Automated [¹⁵O]H₂O Production and Injection System for PET Imaging. *Nucl. Med. Biol.* 22, 241-249.
- Sajjad M, Liow J-S, Zaini MR, Rottenberg DA, Strother SC. 2000. Fast PET scanning for brain activation studies with [¹⁴O]water. *J Nucl Med Supplement* 41:244P.
- Schmand M, Wienhard K, Casey ME, Eriksson L, Jones WF, Reed JH, Treffert J, Lenox M, Luk P, Bao J, Young JW, Baker K, Miller SD, Knoess C, Vollmar S, Richerzhagen N, Flugge G, Heiss WD, Nutt R. 1999. *Conference Record of the 1999 IEEE Nuclear Sciences Symposium and Medical Imaging Conferences (CD-ROM)*.
- Segebarth S, Belle V, Delon C, Massarelli R, Decety J, Le Bas J-F, Decors M, Benabid AL. 1994. Functional MRI of the human brain: predominance of signals from extracerebral veins. *Neuroreport* 5:813-816.
- Silbersweig DA, Stern E, Frith CD, Carhill C, Schnorr L, Crootoonk S, Spinks T, Clark J, Frackowiak RSJ, Jones, T. 1993. Detection of thirty-second cognitive activations in single subjects with positron emission tomography: a new low-dose [¹⁵O]water regional cerebral

blood flow 3D imaging technique. *J Cereb Blood Flow Metab* 13:617-629.

Strother SC, Anderson JR, Xu X-L, Liow J-S, Bonar DC, Rottenberg DA. 1994. Quantitative comparisons of image registration techniques based on high-resolution MRI of the brain. *J Comput Assist Tomogr* 18:954-962.

Strother SC, Anderson JR, Schaper KA, Sidtis JJ, Liow J-S, Woods RP, Rottenberg DA. 1995. Principal component analysis and the scaled subprofile model compared to intersubject averaging and statistical parametric mapping: I. Functional connectivity of the human motor system studied with [¹⁵O]water PET. *J Cereb Blood Flow Metab* 15:738-753.

Strother SC, Sidtis JJ, Anderson JR, Schaper K, Rottenberg DA. 1996. [¹⁵O]water PET: More "noise" than Signal? In: Jones T et al., editor. *Quantification of Brain Function using PET*. San Diego:Academic Press, P378-383.

Tegeler C, Strother SC, Anderson JR, Kim S-G. 1999. Reproducibility of BOLD-based functional MRI obtained at 4T. *Human Brain Mapping* 7:267-283.

Turner R, Howseman A, Rees G, Josephs O. 1997. Functional Imaging with Magnetic Resonance. In: Frackowiak RSJ et al., editor. *Human Brain Function*. San Diego:Academic Press, P467-486.

Toga AW, Frackowiak RSJ, Mazziotta JC, editor. 1999. *Methods, physiology and cognition; fifth International Conference on Functional Mapping of the Human Brain*. *Neuroimage* 9:S1-S400.

Woods, RP, Grafton, ST, Holmes CJ, Cherry SR, Mazziotta JC. 1998. Automated image registration: I. General methods and intrasubject, intramodality validation. *J Comput Assist Tomogr* 22:139-152.

Wu H-M, Huang SC, Vivekanand A, Wolfenden PJ, Schelbert HR. 1996. Derivation of input function from FDG-PET studies in small hearts. *J Nucl Med* 37:1717-1722.

Zaini R, Strother SC, Anderson JR, Liow J-S, Kjems U, Tegeler C, Kim S-G. 1999. Comparison of matched BOLD and FAIR 4.0T-fMRI with [¹⁵O]water PET brain scans. *Med Phys* 26:1559-1567.

FIGURE CAPTIONS

Figure 1. Timetable for tracer delivery, task execution and acquisition of a run containing 9 x 10 sec scans.

Figure 2. Two slices from eigenimages associated with PC2 (top row) and PC3 (bottom row) of Subject 5 after PCA. Scans were pre-processed with standard alignment and without normalization. Black, gray and white represent negative, zero and positive weights respectively.

Figure 3. Principal components 1-6 after PCA of images from Subject 5 pre-processed with consensus alignment and volume mean normalization (VMN). Eigenvector weights of individual 10 sec scans from the four activation and the four control runs are plotted on the left (1-9) and on the right (10-18) of each panel, respectively.

Figure 4. Principal components 1-6 after PCA of images from Subject 5 pre-processed with consensus alignment and without normalization. Eigenvector weights of individual 10 sec scans from the four activation and the four control runs are plotted on the left (1-9) and on the right (10-18) of each panel, respectively.

Figure 5. Selected slices of eigenimages from (A) PC1, (B) PC2 (top row) and PC3 (bottom row) in Fig. 4. PC1 is displayed with a hot-metal color scale because it is all positive, with range: 0.005 (black - orange) to 0.014 (yellow orange - white). For PCs 2 and 3 (range: -0.038 to 0.025), red represents positive (voxel values > 95th percentile) and green represents negative (voxel values < 5th percentile).

Figure 6. The mean eigenvector weights of PC1 calculated across all six subjects (symbols) and their range (shaded band). The 10 sec scans from the activation and control runs are plotted on the left (1-9) and on the right (10-18) of the graph, respectively.

Figure 7. Mean canonical variables (CVs) calculated across 4 x 10 sec scans from repeated activation (1-9, left) and control (10-18, right) bolus time-series (symbols), and their range (shaded band) are plotted for each subject. A canonical variable analysis (CVA) was applied to principal components 2-10 from PCA of non-normalized image volumes with consensus alignment.

Figure 8. Selected slices of canonical eigenimage volumes from CV1 (top row) and CV2 (bottom row) of Subject 5 in Fig. 7. Red represents positive (voxel values > 95th percentile) and green represents negative (voxel values < 5th percentile).

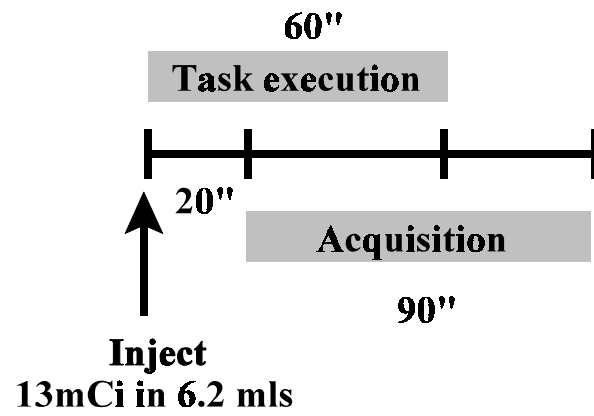


Figure 1

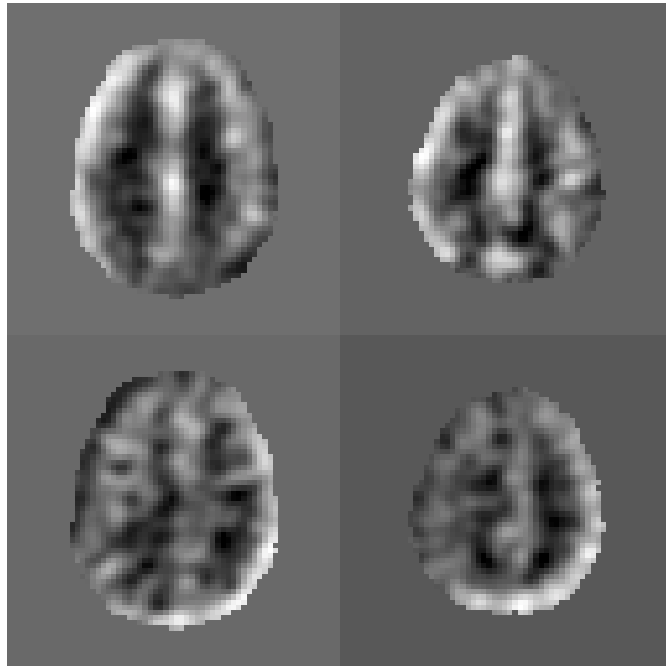


Figure 2

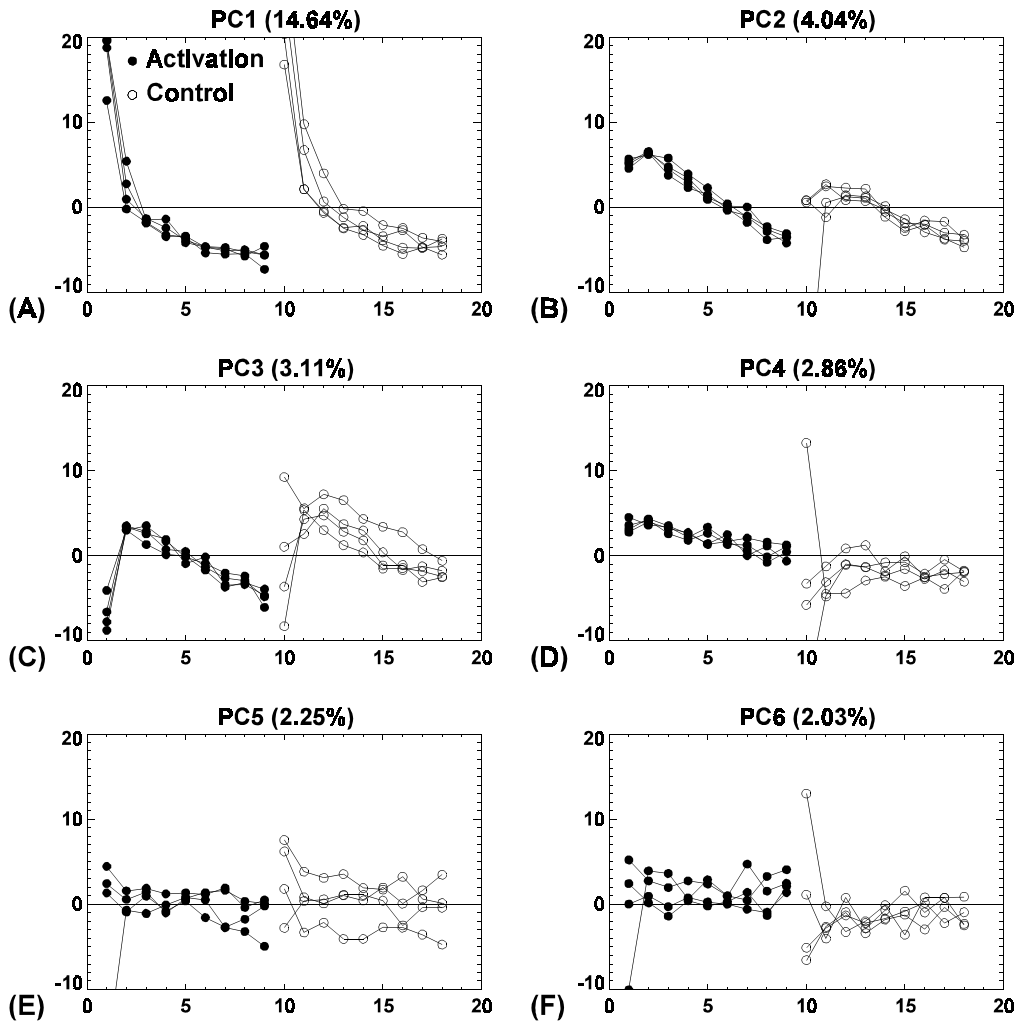


Figure 3

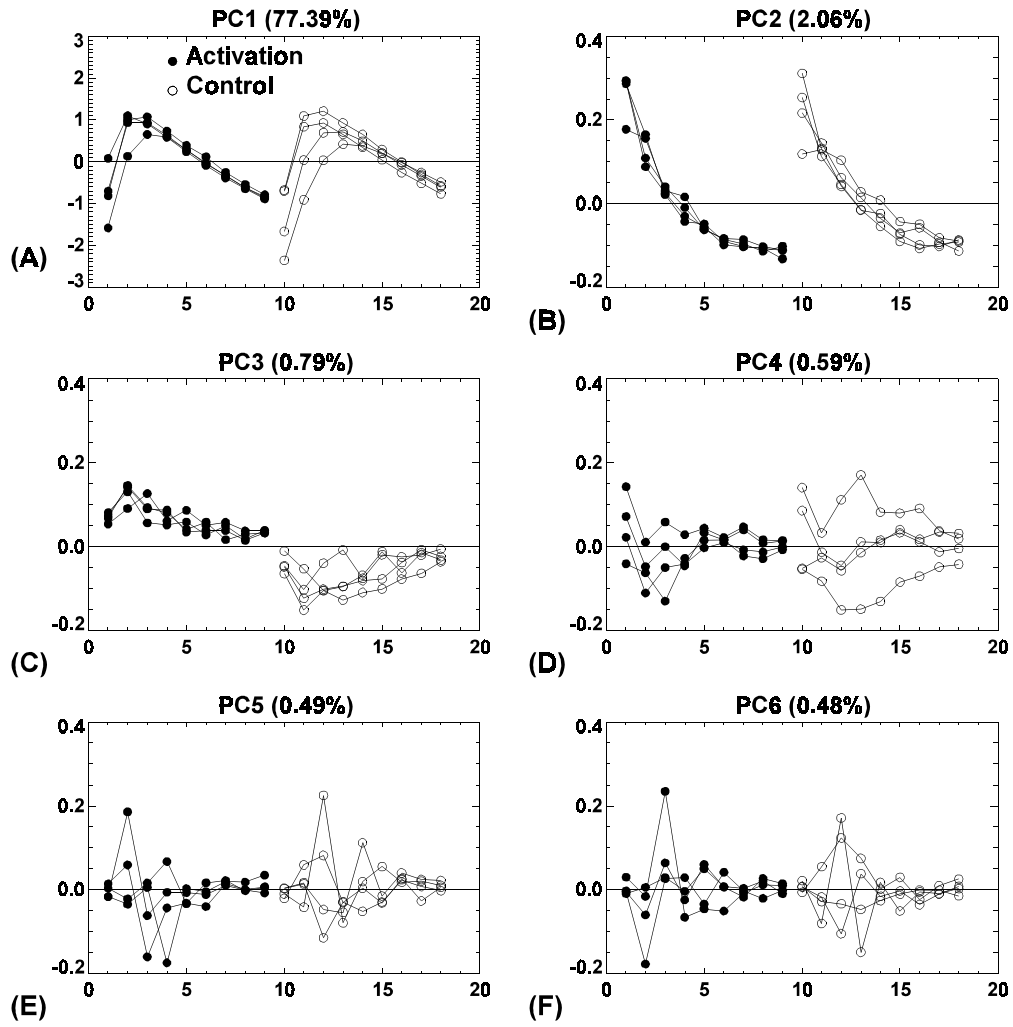
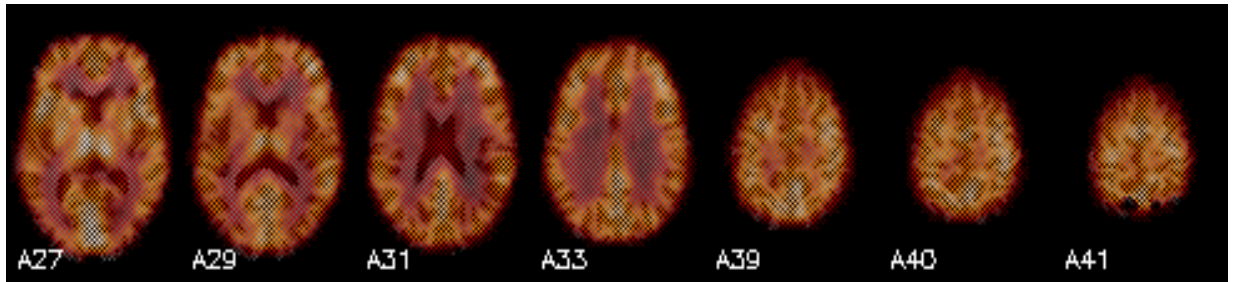
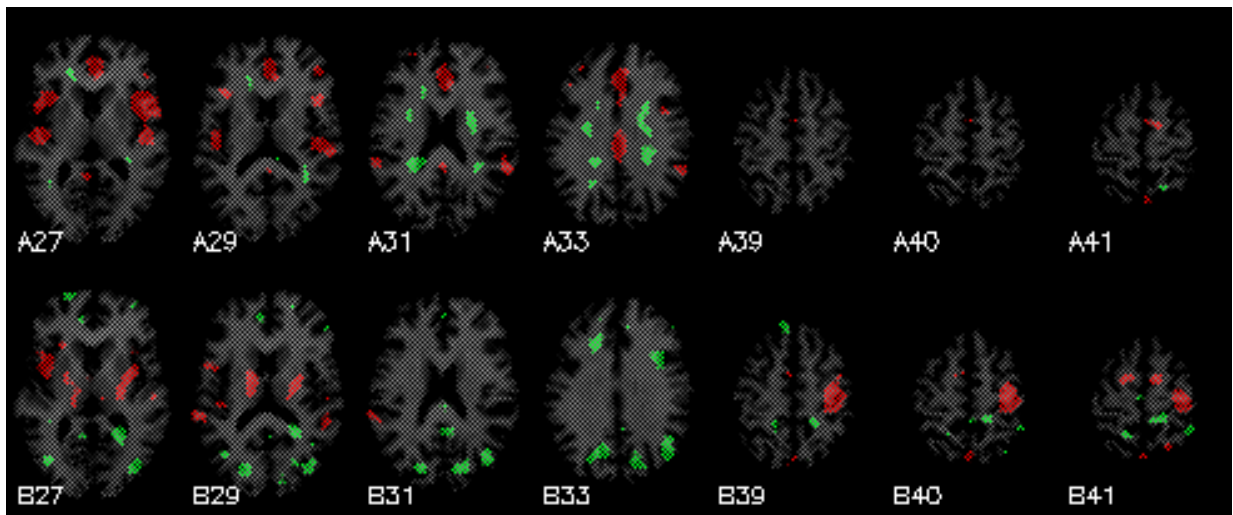


Figure 4



(A)



(B)

Figure 5

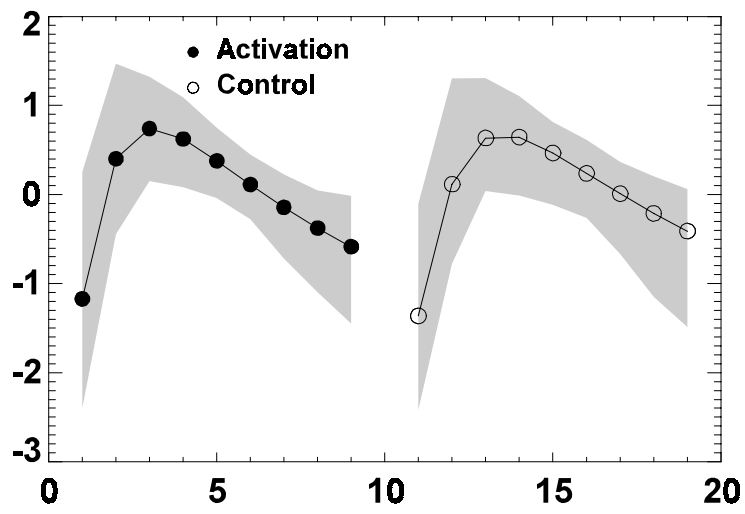


Figure 6

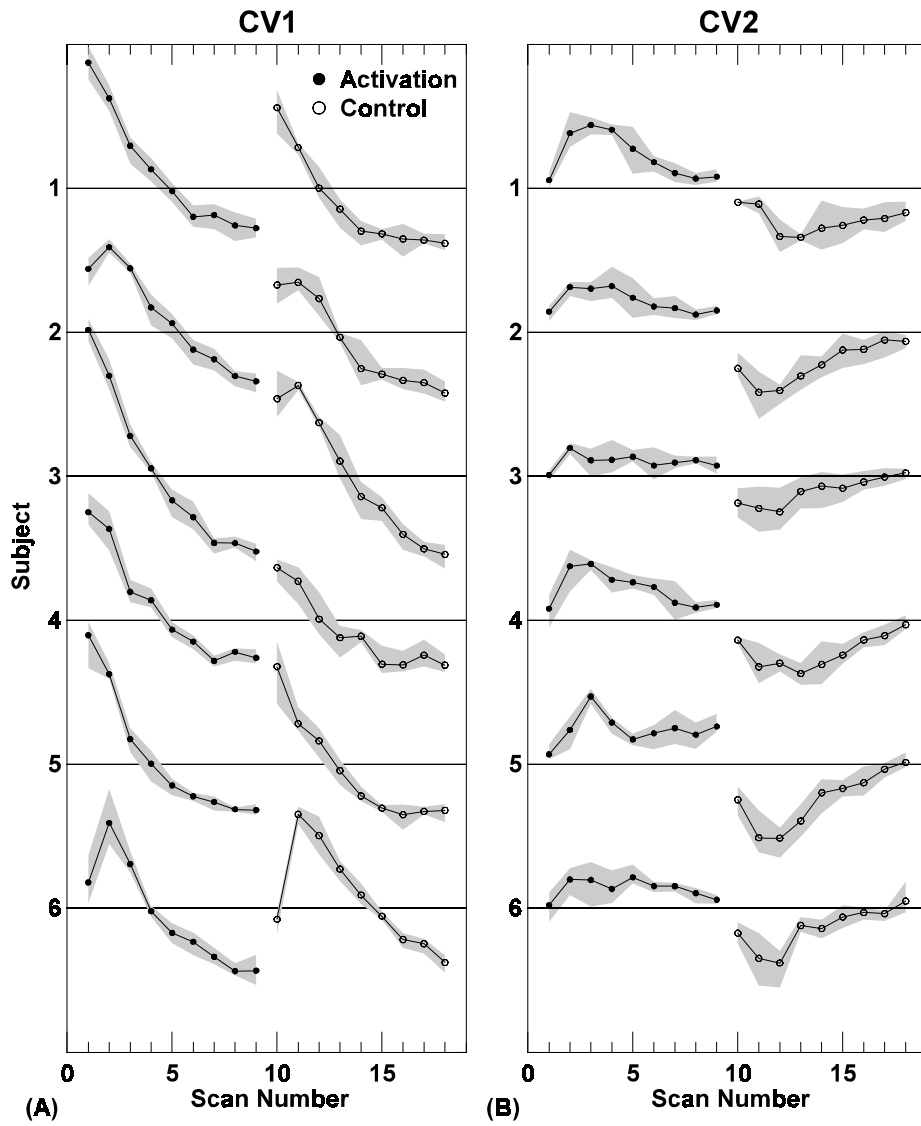


Figure 7

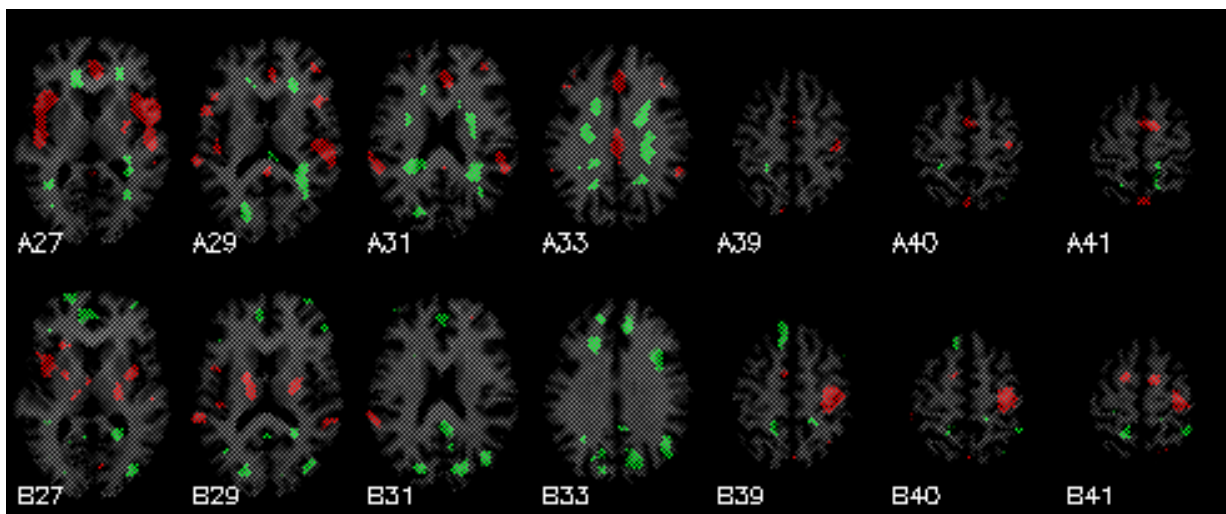


Figure 8